2011 50th IEEE Conference on Decision and Control and
European Control Conference (CDC-ECC)
Orlando, FL, USA, December 12-15, 2011

3-D tracking of fluorescent nanoparticles in a confocal microscope

Zhaolong Shen and Sean B. Andersson
Department of Mechanical Engineering, Boston University, Boston, MA 02215. {zlshen,sanderss}@bu.edu

Abstract— **A system for tracking fluorescent particles in three dimensions based on a standard confocal microscope is described. The method scans the detection volume of the microscope through a six-point measurement pattern, estimates the position of the particle from the measurements, and uses a linear optimal controller to regulate the distance between the center of the measurement pattern and the position of the particle. Experimental results on tracking freely diffusing quantum dots are presented and show good agreement to estimates calculated from CCD images captured during the tracking process.**

I. Introduction

Single-molecule methods relying on particle tracking have become vital tools for the study of systems in molecular biology (see, e.g. [1]). For systems that are confined to a thin layer, such as a cell membrane, two-dimensional (2-D) trajectory information is sufficient for the study of the process dynamics. In many cases, however, the motion is truly three-dimensional (3-D) and the dynamics can only be interpreted by taking the axial motion into account [2].

To acquire such information, several different 3-D particle localization algorithms and tracking methods have been introduced. Many use images captured by a charge-coupled device (CCD) camera. The planar position of the particle can be localized from a camera image using a variety of algorithms, such as the centroid method, [3], Gaussian fitting [4] or similar numerical schemes [5]. The axial position of the particle can also be estimated from the image using different methods, including introducing astigmatism into the optics [6], taking advantage of the details of an out-of-focus image, [7], [8] or using angled micromirrors to project different views of the particles into the image [9]. The temporal resolutions of these methods are typically limited by the need to assure good signal-to-noise ratio (SNR) and the fact that the image processing is computationally complex. Furthermore, these methods are often limited to particles moving near the focal plane.

In recent years, alternative techniques based on confocal microscopy have been introduced. The confocal setup provides true 3-D discrimination and a better SNR than the wide-field setting. In one approach, the excitation laser was split and focused into two planes [10]. Each of these foci was circularly scanned at different rates, encoding the particle position in the fluctuations of the intensity collected by the photon detectors. A feedback controller was implemented to move a nanopositioning stage and regulate the distance between the scanning center and the particle. Other schemes, such as [11]–[13], avoided the need for scanning the detection volume by using multiple photon detectors. All of these schemes require modifications to the standard confocal setup.

In this article, we describe a 3-D particle tracking system that is composed of a standard confocal microscope. The work builds upon an earlier implementation for 2-D tracking [14]. Our implementation uses a stage-actuated system, though the application of the algorithm to a beam-steered system is straightforward. The algorithm first moves the detection volume through a constellation of six measurement locations and then estimates the location of the fluorescent particle from these measurements using the fluoroBancroft (FB) algorithm developed by one of the authors [15]. A linear quadratic Gaussian controller then regulates the distance between the measurement constellation center and the particle. The algorithm is demonstrated through experiment by tracking freely-diffusing quantum dots. Tracking is verified by introducing a beam splitter in the output path of the microscope, focusing some of the signal on a CCD camera, and using a combination of the centroid and radial projection algorithms to estimate the 3-D position of the particle from each image. The 3-D setting provides two main challenges with respect to the 2-D system. First, the model used for position estimation is not as accurate in 3-D, leading to a bias in the FB estimates that needs to be corrected. Second, the dynamics of the piezoelectric state were quite slow in the z–direction, limiting the speed of tracking.

II. Confocal tracking microscope

A. Physical setup

The tracking confocal microscope hardware, shown in Fig. 1, consisted of a standard confocal microscope with a combined digital signal processing (DSP) and field programmable gate array (FPGA) card (Innovative Integrations P25M) for algorithm implementation. A 488 nm laser (ChromaLASE, Blue Sky Research) was spatially filtered by first launching it into an optical fiber, collimating the light out of the fiber, passing it through a 5 μm pinhole and then expanding it to fill the back aperture of the objective lens (water immersion, 63x, 1.2 N.A. C-Apochromat, Carl Zeiss,). The beam was directed into the objective lens using a dichromatic filter (T495LP, Chroma) and focused into the sample. The sample was placed on a 3-D piezoelectric nanopositioning stage (Nano-PDQ, Mad City Labs). The resulting fluorescence was collected by the same objective lens, passed through the dichroic filter and then through a bandpass filter (HW625/30m, Chroma) to separate the excitation signal from the output. The output fluorescence was split into two beams using a beamsplitter. A fraction

978-1-61284-799-3/11/$26.00 ©2011 IEEE

R (33%) was focused onto a CCD camera (Retiga EXi, QImaging). The remaining signal was focused through a 25 μm pinhole and onto the detector of an avalanche photodiode (APD) (SPCM-AQR-14, Perkin Elmer). The output pulses of the APD were counted for an integration time T_{int} by a programmable counter implemented in the FPGA. At each step of the tracking algorithm (c.f. Sec. II-B), the nanopositioning stage was moved through a constellation of six points. At each location, the stage position was sampled by the DSP from the position sensors of the nanopositioning stage and the CCD camera was triggered to capture an image. The nanopositioning stage was operated in a manufacturer-designed closed-loop mode to ensure accurate motion of the sample to the commanded positions. The closed-loop bandwidth of the stage was (120,70,40) Hz in (x, y, z).

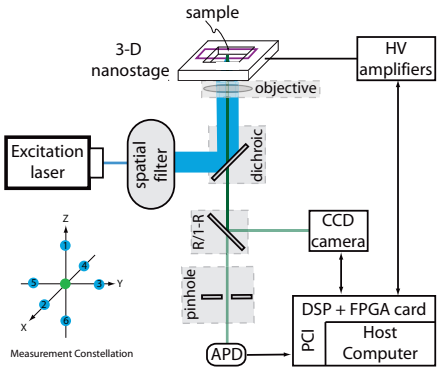

Fig. 1. The confocal tracking microscope. A nanopositioning stage moved the sample through a collection of six locations (lower left). The fluorescence intensity was measured at each position and the collection used to estimate the particle position. An LQG controller regulated the distance between the center of the measurement constellation and the position of the particle. For initialization and tracking verification, a fraction R of the output light was sent to a CCD camera.

B. Control algorithm

As the control algorithm has been previously described [14], we give here only a brief overview. Note that this work uses a straightforward extension of the previous algorithm from 2-D to 3-D. The closed-loop dynamics of the stage were modeled as a linear time-invariant second-order system with parameters identified using the step response of the stage. The motion of the particle was modeled as 3-D diffusion and its position was assumed to be given by a noisy measurement. A linear quadratic Gaussian (LQG) controller was designed for the combined system of the stage and the particle. At each time step of the control algorithm, the stage was moved through a six-point constellation and the fluorescence intensity measured at each position for a fixed integration time. From these measurements, the position of the particle was estimated using the fluoroBancroft (FB) algorithm (see Sec. II-C.1 below) and passed to the LQG controller. The controller then filtered the estimate using a Kalman filter and solved for the control value that minimized a quadratic cost criterion consisting of two terms, the squared error between the controller and the particle, and the cost of control.

The controller depended on seven user-defined parameters: the controller update rate (f_{LQG}), the assumed diffusion coefficient of the particle, D, the weight of the cost of the position error (λ_e), the weight on the cost of control (λ_u), and the diagonal entries of the covariance of the measurement noise, Σ (a diagonal 3×3 matrix under the assumption of independent measurement noise in the three directions).

C. Position estimation

1) FB localization algorithm : We give here a brief description of the FB localization algorithm [15]. The FB algorithm is a model-based localization scheme based on an approximation of the point spread function (PSF) of a microscope by a Gaussian function [16], that is

$$I_{PSF}(x,y,z) = me^{-\frac{(x-x_o)^2}{2\sigma_x^2}-\frac{(y-y_o)^2}{2\sigma_y^2}-\frac{(z-z_o)^2}{2\sigma_z^2}} \tag{1}$$

where $(\sigma_x,\sigma_y,\sigma_z)$ are the widths of the PSF in the three axes and(x_o,y_o,z_o) is the position of the source particle. Given a collection of measurements taken at different positions, the FB algorithm is an analytical expression that essentially calculates a least-squares estimate of the source location. Define the scaling matrix $T = \mathrm{diag}\,(\sigma/\sigma_x, \sigma/\sigma_y, \sigma/\sigma_z)$, where σ is an arbitrary spread, and with it define the scaled coordinates

$$\begin{bmatrix} x' \\ y' \\ z' \end{bmatrix} = T \begin{bmatrix} x \\ y \\ z \end{bmatrix}, \quad \begin{bmatrix} x'_0 \\ y'_0 \\ z'_0 \end{bmatrix} = T \begin{bmatrix} x_o \\ y_o \\ z_o \end{bmatrix}. \tag{2}$$

Given a collection of n measurements, I_i, of the intensity taken at different positions (x_i,y_i,z_i), the closed-form expression for the FB estimate of the source location is given by

$$[\hat{x}_o\,\hat{y}_o\,\hat{z}_o]^T = T^{-1}QB^{\dagger}\alpha, \tag{3}$$

where the components of the vector α are given by

$$\alpha_i = \frac{1}{2}(x_i'^2 + y_i'^2 + z_i'^2) + \sigma^2 \ln(I_i - N_B),$$

with N_B the expected value of the background fluorescence intensity. Here $B^{\dagger} = (B^TB)^{-1}B^T$ and B and Q are given by

$$B = \begin{bmatrix} x'_1 & y'_1 & z'_1 & 1 \\ \vdots & \vdots & \vdots & \vdots \\ x'_n & y'_n & z'_n & 1 \end{bmatrix}, Q = \begin{bmatrix} 1 & 0 & 0 & 0 \\ 0 & 1 & 0 & 0 \\ 0 & 0 & 1 & 0 \end{bmatrix}.$$

In practice, modeling error due to the Gaussian approximation to the actual PSF gives rise to a bias in the FB estimate (see [17] for a theoretical analysis). As described in Sec. II-C.2 below, a user-selected correction term is therefore added to the estimate. That is, (3) is replaced by

$$\begin{bmatrix} \hat{x}_o & \hat{y}_o & \hat{z}_o \end{bmatrix}^T = T^{-1}QB^{\dagger}\alpha + \begin{bmatrix} \delta_x & \delta_y & \delta_z \end{bmatrix}^T. \tag{4}$$

In this work, the measurement constellation was fixed to the six-point structure shown in Fig. 1 and the arbitrary spread σ was set to σ_x. Six is sufficient for accurate estimation (as illustrated by the experimental results in Sec. II-C.2). Additional measurement points can be used to increase

estimation accuracy, particularly in low SNR settings, at the cost of slowing the tracking algorithm.

The FB algorithm depends on nine user-defined parameters: the integration time at each measurement location (T_{int}), the radius of the measurement pattern (r), the background rate (N_B), the spreads of the Gaussian approximation to the PSF (σ_x, σ_y, σ_z), and the corrections (δ_x, δ_y, δ_z).

2) Centroid and radial projection algorithms: To provide an initial position and an independent measurement of the particle position in 3-D, the radial projection method [18] was used. The CCD camera was triggered to take a snapshot at each measurement location and the planar position of the fluorescent particle was estimated using the centroid method,

$$(x_c, y_c) = \left(\sum I_i x_i / \sum I_i, \sum I_i y_i / \sum I_i\right), \tag{5}$$

where (x_i, y_i) is the pixel position in the image and I_i is the corresponding pixel intensity value. The axial position is calculated from the 2-D image by taking advantage of the fact that the 2-D image of a particle is circularly symmetric and thus can be described by a 1-D radius vector. The radius vector of an image is calculated by determining the average intensity of the pixels at pre-specified distances from the center (as determined by 2-D localization). The radius vector is then compared against a calibration set to determine the axial position. In this work, the calibration set was calculated from a collection of 900 images of fixed quantum dots acquired at 5 nm intervals along the optical axis.

The control algorithm was implemented in the DSP card and a graphical user interface (GUI) was created to load parameters, communicate with the DSP card, and save and display the tracking results in real time. Samples were prepared by diluting a solution of quantum dots (QD625, Invitrogen) in a glycerol/water solution. The diffusion coefficient of the quantum dots was varied by adjusting the weight ratio of the glycerol/water solution. A small amount of the solution was placed on a glass slide and sealed with a cover slip. The slide was mounted on the nanostage and visually searched to find an isolated quantum dot in the preview window of the camera. A particular quantum dot was selected by clicking on it with the mouse of the computer. The system then acquired a CCD image and estimated the planar position of the particle using the centroid method. Due to the time to execute the radial projection algorithm, the axial position was not estimated but simply set to the center of the range. This position was then sent to the DSP, together with all controller parameters, and used to initialize the tracking procedure. All measured data, including the nanostage positions, photon counts and the CCD images, were sent back to the computer for displaying the tracking in real-time, saving, and off-line analysis.

Several parameters were set to the same value in all experiments with the choices shown in Table II-C.2. In all experiments, the weights (λ_e, λ_u) for the LQG controller reflected the fact that there was little cost to changing the control signal. The background rate N_B was determined based on measurements with the confocal microscope from a region with no quantum dots. The radius r of the measurement pattern was selected based on a prior analysis of the FB algorithm [19] while the integration time T_{int} was set as long as possible within the update rate of the controller. Other parameters were changed in different experiments; their selection is described below.

Parameter	value	Parameter	value
λ_e	1000	λ_u	0.001
N_B	0 counts	r	$\sqrt{2}\sigma$ nm
T_{int}	2 ms	T_{CCD}	20 ms

The rsegion-of-interest of the camera was set to the center 64×64 pixels. Since only 1/3 of the output light was directed to the CCD, the measured intensity on the camera was quite low with peak intensities between 7-12 counts. As a result, the accuracy of the CCD-based position estimates was quite poor (c.f. Figs. 2, 3). Nevertheless, these estimates serve as a baseline based on a well-accepted localization algorithm.

D. Tracking a fixed particle

The system was first tested using a fixed quantum dot. The LQG update rate was set to $f_{LQG} = 5$ Hz and thus the rate through the measurement constellation was 30 Hz. The noise covariance Σ was set based on prior experience to correspond to a standard deviation in the FB estimate of 20 nm in the planar directions and 50 nm along the optical axis. While it was known *a priori* that the quantum dot was fixed, a value of $D = 0$ μm^2/s in the algorithm would significantly slow the convergence of the controller. Thus the diffusion coefficient was set to $D = 1\times10^{-5}\mu$m^2/s. The spreads and corrections in the FB algorithm were manually selected so as to balance the measured average fluorescence intensities at each of the measurement locations, leading to $(\sigma_x, \sigma_y, \sigma_z) = (133, 129, 545)$ nm and $(\delta_x, \delta_y, \delta_z) = (35, 60, 10)$ nm.

A typical experimental result is shown in Fig. 2. The particle position estimates are shown in Fig. 2(a-c). The center line (red) is the position as determined by the tracking algorithm, the intermediate dots (blue) are the raw position estimate generated by the FB algorithm, and the noisiest line (green) is the estimate derived from the centroid/radial projection approach. For the run shown, the standard deviation in the (x, y, z) position estimates for the tracking algorithm, raw FB estimates, and from the centroid/radial projection algorithm from the CCD images were

$$\begin{aligned} (5.9, 8.5, 14.5)\,\text{nm} \quad & \text{(tracking algorithm)}, \\ (11.9, 13.1, 42.2)\,\text{nm} \quad & \text{(FB)}, \\ (63.4, 102, 253)\,\text{nm} \quad & \text{(CCD)}. \end{aligned}$$

The increased variance in the y direction relative to x is likely due to modeling errors between the theoretical and true PSF and misalignment of the excitation source, leading to coupling between the z and y directions. The offset n the z direction of the radial projection method relative to the other is due to a difference in the definition of the zero position. The FB and tracking algorithm estimates are relative to a lab frame defined by the nanopositioning stage while the radial projection algorithm is defined relative to a frame defined by the calibration procedure.

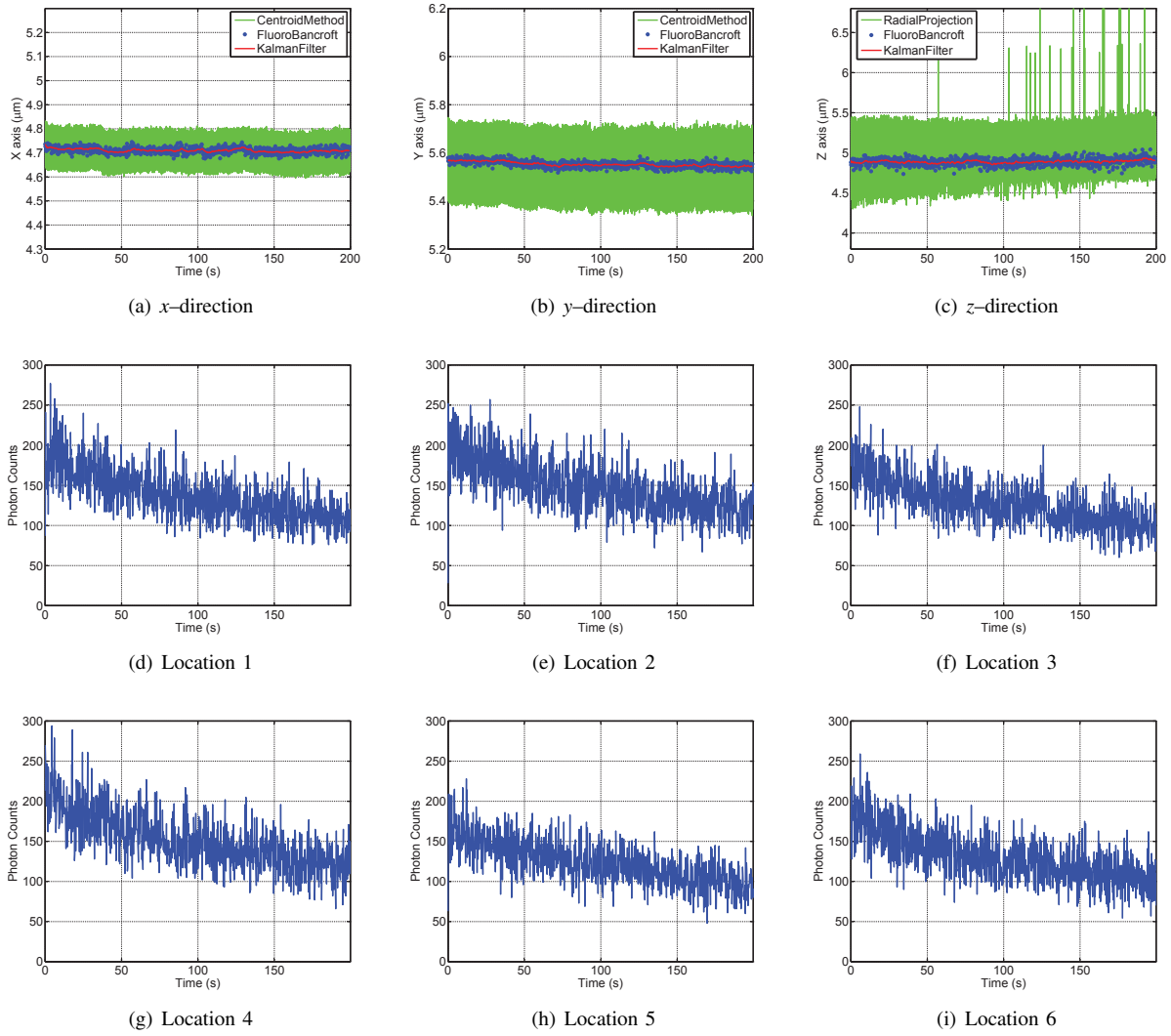

(a) x–direction (b) y–direction (c) z–direction

(d) Location 1 (e) Location 2 (f) Location 3

(g) Location 4 (h) Location 5 (i) Location 6

Fig. 2. Tracking run with a fixed particle. (a-c) Position estimates from the tracking algorithm (center line,red), the raw FB estimates (intermediate dots, blue), and the centroid/radial projection algorithm (noisiest line, green). The poorer performance of these last estimates is due to the low intensity at the CCD camera. (d-i) Fluorescence intensity measurements at the six measurement locations ranged from approximately 180 counts/2 ms (90,000 counts/sec) at the beginning of the experiment to 100 counts/2 ms (50,000 counts/sec) after 200 seconds of tracking.

The intensities at the six measurement locations are shown in Fig. 2. As expected, all six show very similar results with a decay in signal level over the duration of the experiment due to slow photobleaching of the quantum dot. At the beginning of the experiment, the average signal level at each location was approximately 180 counts/2 ms (90,000 counts/s) while after 200 s the level had decayed to approximately 100 counts/2 ms (50,000 counts/s).

E. Tracking Single Diffusing Particles

To prepare a diffusing particle, a small amount of the sample solution was put into a well on a microscope slide such that the quantum dots could freely diffuse in the wells. The well was then sealed with a cover slip. Because the quantum dots were away from the coverslip boundary, the shape of the PSF changed relative to that in the fixed particle experiments, necessitating changes to the FB parameters. To do this, a slowly diffusing particle was chosen and the parameters of the FB algorithm were once again selected so as to balance the measured intensities at each of the six measurement locations, leading to $(\sigma_x, \sigma_y, \sigma_z) = (114, 108, 482)$ nm and $(\delta_x, \delta_y, \delta_z) = (35, 50, 30)$ nm.

The true value of the diffusion coefficient value D was unknown in each experiment because both the experimental temperature and the sample preparation procedure were not strictly controlled. It was also possible that individual particles could be small aggregations of quantum dots and as a result the diffusion coefficient could not be accurately estimated using the Stokes-Einstein equation. Given a particle trajectory, however, the diffusion coefficient can be estimated from the mean-square displacement (MSD) of that trajectory,

$$MSD(\tau) = \langle (\hat{x}_p(t) - \hat{x}_p(t+\tau))^2 + (\hat{y}_p(t) - \hat{y}_p(t+\tau))^2 + (\hat{z}_p(t) - \hat{z}_p(t+\tau))^2 \rangle = 6D\tau,$$

where $(\hat{x}_p(t), \hat{y}_p(t), \hat{z}_p(t))$ is the estimated particle trajectory

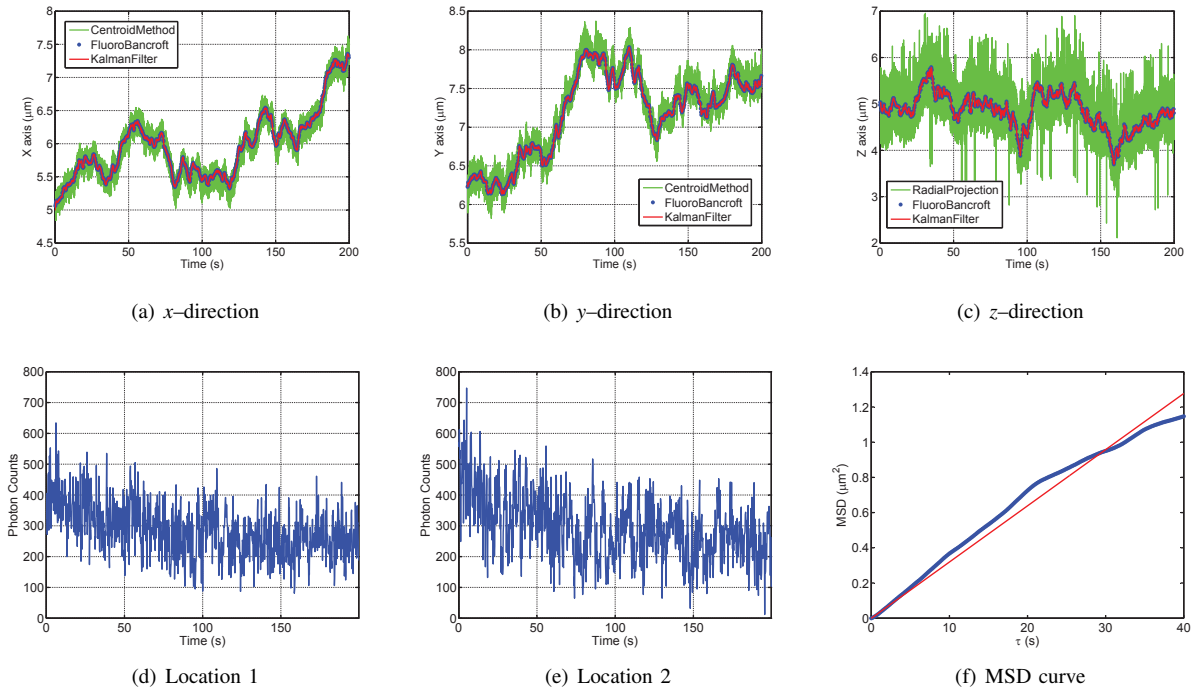

(a) x–direction (b) y–direction (c) z–direction

(d) Location 1 (e) Location 2 (f) MSD curve

Fig. 3. Tracking run with a slowly diffusing particle. (a-c) Position estimates from the tracking algorithm (center line,red), the raw FB estimates (intermediate dots, blue), and the centroid/radial projection algorithm (noisiest line, green). (d-e) Fluorescence intensity measurements at the first two measurement locations (traces from the remaining four were similar and are omitted) (f) MSD curve and linear fit yielding $D = 0.005$ μm^2/s.

[20]. Thus, after preparing a solution, a few trial runs were made, the diffusion coefficient was estimated from the MSD curves, and then this value was used in the controller for subsequent runs. (For a discussion of the impact of errors in the value of D on tracking, see [14].) The amount of time for a tracking run was set *a priori* by the user.

1) Sample Run With Low Diffusion: In order to track a slowly diffusing particle, the LQG update rate was again set to 5 Hz. The noise covariance Σ was increased along the optical axis to 60 nm since the slow diffusion was expected to have little effect on the planar estimate but lead to reduced performance in the axial direction. The value of D in the LQG controller was set to 0.007 μm^2/s. The results of a typical tracking run are shown in Fig. 3. The trajectory is shown in Fig. 3(a-c) where, as with the fixed particle, the tracking algorithm estimates are the center line (red), the raw FB estimates are the intermediate dots (blue), and the centroid/radial projection results are the noisiest line (green). As with the fixed particle case, all three estimates produce similar results with the noisiest estimates in the z direction. The measured fluorescence counts at locations one (above the estimated particle position) and two (in the plane of the estimated particle position) are shown in Fig. 3(d-e). (Measurements from the remaining four positions were similar and are omitted for space reasons.) While the tracking algorithm held the measured signal relatively constant, apart from a slow decay due to photobleaching, there is clearly an increased variance relative to the fixed particle case arising from the diffusion of the particle. The average measured intensity over the course of the tracking run was 302 counts/2 ms (151,000 counts/s). The MSD curve for the tracking run is shown in Fig. 3(f), yielding $D = 0.005$ μm^2/s.

2) Sample Run With Faster Diffusion: To track faster diffusing particles, the rate of the LQG controller was increased to 8 Hz, corresponding to a scanning rate around the measurement constellation of 48 Hz. At this higher rate, the exposure time needed on the CCD camera to collect sufficient intensity for reasonably accurate estimation was too long and thus no CCD images were acquired. The noise covariance Σ was increased to 40 nm in the planar directions and 80 nm along the optical axis to account for the effect of diffusion during the acquisition of the intensity measurement. The diffusion coefficient in the LQG controller was set to $D = 0.1$ μm^2/s. Results from a typical run are shown in Fig. 4. The trajectory is shown in Fig. 4(a-c) with the tracking algorithm estimates shown as a solid (red) line and the raw FB estimates as (blue) points. For space reasons, the measured intensities are omitted. The intensities showed a significantly higher variance than when a more slowly diffusing particle was tracked. The average intensity over the course of the run was 197 counts/2 ms (98,500 counts/s).

The tracking time was set to 25 seconds due to the order of magnitude increase in the diffusion coefficient. (Note that tracking did not fail at the completion of the run.) This time should be compared to the expected first passage time out of the confocal detection volume with dimensions defined by $(\sigma_x, \sigma_y, \sigma_z)$ [21]. For a value of $D = 0.11$ μm^2/s, this time is approximately 30 ms.

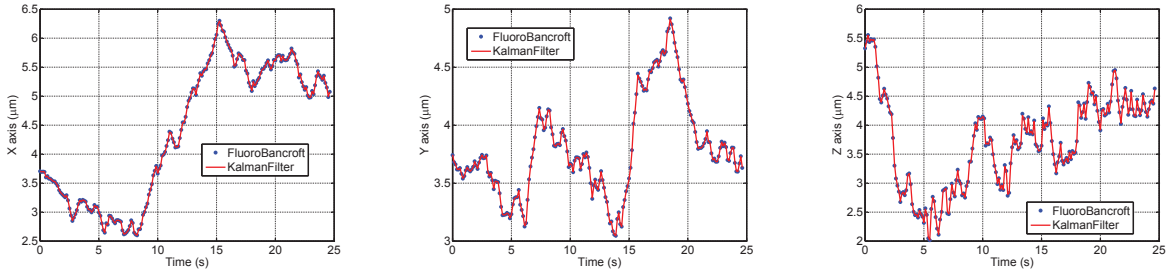

(a) x–direction (b) y–direction (c) z–direction

Fig. 4. Tracking run with a faster diffusing particle. (a-c) Position estimates from the tracking algorithm (center line,red), the raw FB estimates (intermediate dots, blue), and the centroid/radial projection algorithm (noisiest line, green). (d-e) Fluorescence intensity measurements at the first two measurement locations (traces from the remaining four were similar and are omitted) (f) MSD curve and linear fit yielding $D = 0.11\ \mu\text{m}^2/\text{s}$.

III. Conclusions

In this paper, a confocal tracking microscope was demonstrated through experiments for tracking nanometer-scale fluorescent particle in real-time. For lower values of the diffusion coefficient, tracking results were verified using offline position estimation based on CCD images captured during the experiments. Under our approach, the system is easily extended to tracking multiple particles by either simply time-sharing the controller between different particles [14] or by taking advantage of results from networked control systems to optimize the time spent on each particle [22].

As is any single particle tracking scheme, performance involves a tradeoff in the number of photons collected (and thus the measurement integration time for a fixed excitation intensity) and the rate of the controller updates. At the loop rates dictated by the bandwidths of the stage controllers, the system is able to collect a relatively large number of photons. Thus, the primary limitation of the current setup are the slow dynamics of the nanopositioning stage.

IV. Acknowledgements

This work was supported in part by the National Science Foundation through DBI-0649823 and CMMI-0845742.

References

[1] W. E. Moerner, "New directions in single-molecule imaging and analysis," *Proc. Nat. Acad. Sci. USA*, vol. 104, no. 31, pp. 12 596–12 602, July 2007.

[2] Q. Zhang, C. Dang, H. Urabe, J. Wang, S. Sun, and A. Nurmikko, "Large ordered arrays of single photon sources based on ii-vi semiconductor colloidal quantum dot," *Opt. Expr.*, vol. 16, pp. 19 522–19 599, 2008.

[3] M. K. Cheezum, W. F. Walker, and W. H. Guilford, "Quantitative comparison of algorithms for tracking single fluorescent particles," *Biophys. J.*, vol. 81, no. 4, pp. 2378–2388, October 2001.

[4] R. E. Thompson, D. R. Larson, and W. W. Webb, "Precise nanometer localization analysis for individual fluorescent probes," *Biophys. J.*, vol. 82, no. 5, pp. 2775–2783, May 2002.

[5] A. J. Berglund, M. D. McMahon, J. J. McClelland, and J. A. Liddle, "Fast, bias-free algorithm for tracking single particles with variable size and shape," *Opt. Expr.*, vol. 16, no. 18, pp. 14 064–14 075, September 2008.

[6] B. Huang, W. Wang, M. Bates, and X. Zhuang, "Three-dimensional super-resolution imaging by stochastic optical reconstruction microscopy," *Science*, vol. 319, no. 5864, pp. 810–813, January 2008.

[7] H. P. Kao and A. S. Verkman, "Tracking of single fluorescent particles in three dimensions: use of cylindrical optics to encode particle position," *Biophys. J.*, vol. 67, no. 3, pp. 1291–1300, September 1994.

[8] M. Speidel, A. Jonáš, and E.-L. Florin, "Three-dimensional tracking of fluorescent nanoparticles with subnanometer precision by use of off-focus imaging," *Opt. Lett.*, vol. 28, no. 2, pp. 69–71, 2003.

[9] M. D. McMahon, A. J. Berglund, P. Carmichael, J. J. McClelland, and J. A. Liddle, "3d particle trajectories observed by orthogonal tracking microscopy," *ACS Nano*, vol. 3, no. 3, pp. 493–497, 2009.

[10] K. McHale, A. J. Berglund, and H. Mabuchi, "Quantum dot photon statistics measured by three-dimensional particle tracking," *Nano Lett.*, vol. 7, no. 11, pp. 3535–3539, November 2007.

[11] H. Cang, C. M. Wong, C. S. Xu, A. H. Rizvi, and H. Yang, "Confocal three dimensional tracking of a single nanoparticle with concurrent spectroscopic readouts," *Appl. Phys. Lett.*, vol. 88, no. 22, pp. 223 901(1–3), May 2006.

[12] H. Cang, C. S. Xu, D. Montiel, and H. Yang, "Guiding a confocal microscope by single fluroescent nanoparticles," *Opt. Lett.*, vol. 32, no. 18, pp. 2729–2731, September 2007.

[13] G. A. Lessard, P. M. Goodwin, and J. H. Werner, "Three-dimensional tracking of individual quantum dots," *Appl. Phys. Lett.*, vol. 91, no. 22, p. 224106, November 2007.

[14] Z. Shen and S. B. Andersson, "Tracking nanometer-scale fluorescent particles in two-dimensions with a confocal microscope," *IEEE Trans. Cont. Syst. Tech.*, vol. 19, no. 5, pp. 1269–1278, 2011.

[15] S. B. Andersson, "Localization of a fluorescent source without numerical fitting," *Opt. Expr.*, vol. 16, no. 23, pp. 18 714–18 724, November 2008.

[16] D. Thomann, D. R. Rines, P. K. Sorger, and G. Danuser, "Automatic fluorescent tag detection in 3D with super-resolution: application to the analysis of chromosome movement," *J.. Micro.*, vol. 208, no. 1, pp. 49–64, October 2002.

[17] Z. Shen and S. B. Andersson, "Bias and precision of the fluorobancroft algorithm for single particle localization in fluorescence microscopy," *IEEE Tran. Signal Proc.*, vol. 59, no. 8, pp. 4041–4046, 2011.

[18] Z. Zhang and C.-H. Menq, "Three-dimensional particle tracking with subnanometer resolution using off-focus images," *Appl. Opt.*, vol. 47, no. 13, pp. 2207–2214, 2008.

[19] Z. Shen and S. B. Andersson, "Optimal measurement constellation of the fluorobancroft localization algorithm for position estimation in tracking confocal microscopy,," in *5th IFAC Symposium on Mechatronic Systems*, 2010.

[20] M. J. Saxton and K. Jacobson, "Single-particle tracking: applications to membrane dynamics," *Ann. Rev. Biophys. Biomol. Struct.*, vol. 26, pp. 373–399, June 1997.

[21] G. Klein, "Mean first-passage times of Brownian motion and related problems," *Proc.Royal Soc. London A,*, vol. 211, no. 1196, pp. 431–443, March 1952.

[22] D. Hristu-Varsakelis and L. Zhang, "LQG control of networked control systems with access constraints and delays," *Int. J. Cont.*, vol. 81, no. 8, pp. 1266–1280, August 2008.